

Tomographic PTV measurements of a rectangular body wake using spatio-temporal information

Gyeong-rae Cho^{1*}, Dae-keong Kong², Joon-ho Kim², Deog-hee Doh¹

¹ Korea Maritime and Ocean Univ., Division of Mechanical Eng., Busan, Korea

² Graduate School, Korea Maritime and Ocean Univ., Dept. of Refrigeration and Air-conditioning, Busan, Korea

*doh@kmou.ac.kr

Abstract

A new tomographic PTV has been adopted to measure the wakes of a rectangular bluff body using spatio-temporal information of the particles moving with the working fluid. The measurement system consists of 4 sets of high speed camera (1k x 1k). The influences of the self-calibration of camera on the measurement accuracy of the tomographic PTV have been investigated, in which the phantom particle images have been used. Further, the influences of the camera calibration on the calculation accuracy of the particle centroids have been also investigated. Two methods of camera calibrations, 10 parameter method and 11 parameter method (Mapping Function Method), have been tested. After making confirmation of the constructed tomographic PTV approach, measurements have been performed on the rectangular bluff body in Reynolds number 2,000. Instantaneous structures of the wake have been quantitatively reconstructed.

1 Introduction

Since most of the flow phenomena seen in various industry show strong three-dimensional and complex flow aspects, 3D measurement techniques have been developed. Since 3D-PTVs had been reported by Mass et al. (1993) and Malik et al.(1993), there had been many attempts to use the 3D-PTVs for three-dimensional flow measurements. However, since the number of vectors obtained from 3D-PTV measurements was within several thousands, it had not been widely used in various application. In order to increase the number of vectors, stereoscopic PIV(SPIV) was proposed by Arroyo and Greated (1991). However, the measurements results by SPIV are restricted to 2D plane. To extend to 3D volume from 2D plane with highly number of vectors, digital holography PIV (HPIV) was proposed by Meng and Hussain (1991). The number of instantaneous vectors obtained by HPIV was a few millions. Unfortunately, HPIV is very sensitive to the optical apparatus, which implies that HPIV users are restricted to certain purposes. To overcome this disadvantage of HPIV, tomographic PIV (Tomo PIV) was proposed by Elsinga et al. (2006). Tomo PIV had also a disadvantage at the first type, in which the errors in calculating particles' positions were large and this eventually produced many erroneous vectors in the final vectors. To overcome this issue, Wieneke (2008) proposed a volume self-calibration algorithm. He evaluated the accuracy of the Tomo PIV based on the camera calibration method, 11 camera parameter method, in which a mapping function was adopted using the volume self-calibration algorithm.

In this study, the influences of the camera calibration methods to measurement accuracy of the Tomo PIV or Tomo PTV have been investigated. Two calibration methods, 10 parameter method (Doh et al., 2002)

and 11 parameter method (Wieneke, 2006), have been adopted to this evaluation. After this, measurements have been performed by the constructed Tomo PTV system for the wake of a rectangular bluff body, from which temporal motions of the wake structures have been investigated.

2 Tomographic Measurements

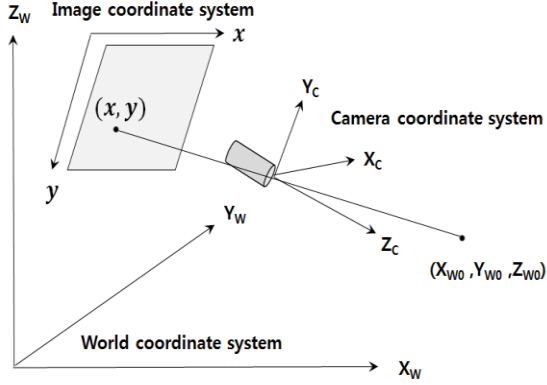


Figure 1: Pinhole camera model(11 parameter)

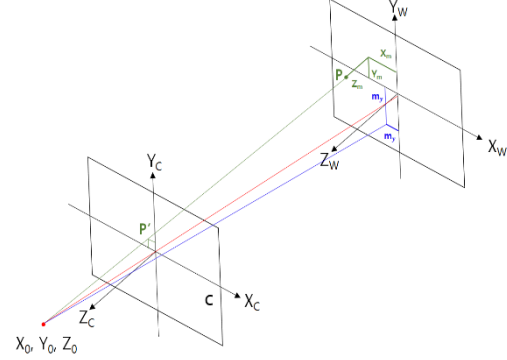


Figure 2: Pinhole camera model(10 parameter method)

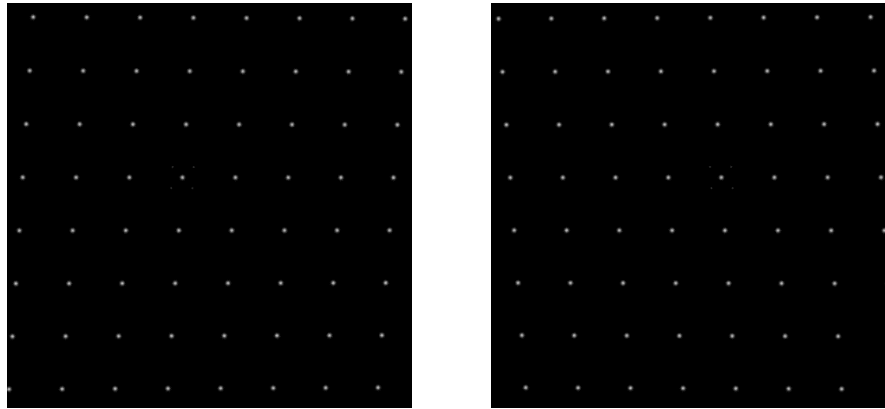
Two camera calibration methods have been adopted. Fig. 1 shows the camera coordinate system for the 11 parameter method (Arroyo, 1991). Fig. 2 shows the camera coordinate system for the 10 parameter method (Doh et al., 2002). The 11 parameter method has been based on Eq. (1) and the 10 parameter method has been based on Eq. (2). For each camera calibration, the camera parameters calculated and obtained by using the phantom images have been compared with the imaginary camera parameters. Table 1 shows the imaginary coordinate of the grid system used for camera calibration. Using this imaginary coordinate, the camera parameters for four cameras have been calculated. Fig. 3 shows the phantom images captured imaginarily by the camera 1 and by the camera 2 for the imaginary coordinate.

$$\begin{bmatrix} X_C \\ Y_C \\ Z_C \end{bmatrix} = \begin{bmatrix} f_x & (skew_c) \cdot f_x & C_x \\ 0 & f_y & C_y \\ 0 & 0 & 1 \end{bmatrix} \begin{bmatrix} r_{11}r_{12}r_{13}t_1 \\ r_{21}r_{22}r_{23}t_2 \\ r_{31}r_{32}r_{33}t_3 \end{bmatrix} \begin{bmatrix} X_W \\ Y_W \\ Z_W \\ 1 \end{bmatrix} \quad (1)$$

$$x = c_x \frac{X_m - m_x}{\sqrt{dis^2 - m_x^2 - m_y^2 - Z_m}} + \Delta x, \quad y = c_y \frac{Y_m - m_y}{\sqrt{dis^2 - m_x^2 - m_y^2 - Z_m}} + \Delta y \quad (2)$$

Table 1: Imaginary coordinate of the grid system

	Minimum[mm]	Maximum[mm]	Gap[mm]
X	-20	20	5
Y	-20	20	5
Z	-10	10	1



(a) by camera 1

(b) by camera 2

Figure 3: Phantom images reconstructed by cameras for the imaginary coordinate

Table 2: Calibration results obtained by the 10 parameter method

Cam	Reference parameter				Calculated parameter			
	1	2	3	4	1	2	3	4
dis	1000	1000	1000	1000	1008.284	1004.792	1003.740	1000.209
c	14000	14000	14000	14000	14114.21	14065.52	14050.58	14001.35
α	0.261799	0.261799	-0.2618	-0.2618	0.261858	0.261866	-0.261853	-0.261862
β	0.261799	-0.2618	0.261799	-0.2618	0.261856	-0.261845	0.261858	-0.261847
γ	0	0	0	0	0.000040	-0.000041	-0.000037	0.000038
m_x	0	0	0	0	0.000470	-0.000303	0.000329	-0.000163
m_y	0	0	0	0	0.000038	0.000152	-0.000099	-0.000213

Table 2 shows the calibration results for the camera 1. The reference parameters were used for generating the phantom images of the imaginary coordinate. Table 2 shows the reference parameters of the camera 1 and the camera parameters calculated by the 10 parameter method (Doh et al., 2002) using the phantom images of the camera 1. The 11 parameter method (Arroyo, 1991) was also tested. It can be read that the reference parameters and the calculated parameters show slight difference each other. This implies that the calculation accuracy for the particle centroids influences the calculation errors for positional data of the particles. All camera parameters for the four cameras have been tested in this manner.

Fig. 4 shows the pixel errors of the camera 1 between the original photographic coordinate of the reference grid data and the calculated photographic grid data that were calculated by the use of the calculated parameters. Fig. 4(a) and Fig. 4(c) show the pixel errors obtained for the x and y coordinate of the reference data for the camera 1 respectively using the 10 parameter method. Fig. 4(b) and Fig. 4(d) show the pixel errors obtained for the x and y coordinate of the reference data respectively using the 11 parameter method. It has been confirmed that the RMS (root mean square) value of the errors calculated by the 10 parameter method was 10 times smaller than those values obtained by the 11 parameter method. This implies that the 10 parameter method is appropriate for three-dimensional measurements.

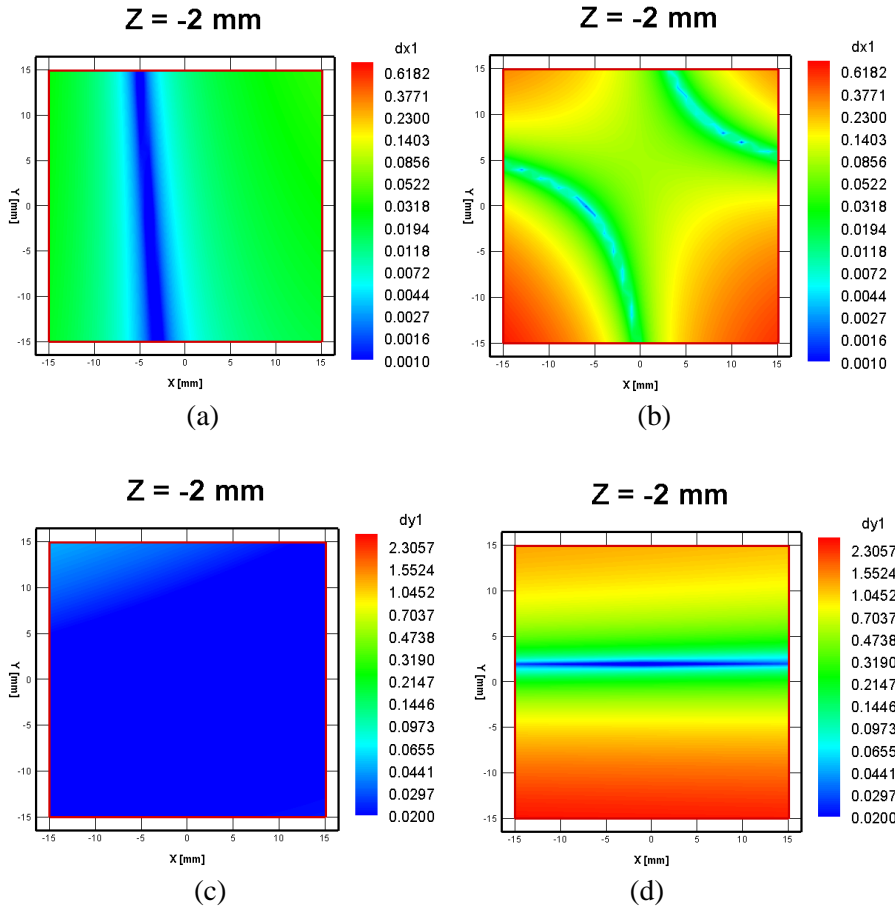


Figure 4: Pixel errors of the camera 1 at $Z=-2\text{mm}$. (a), (c) : 10 parameter method (b), (b): 11 parameter methods

3 Tomographic Measurements

3.1 Numerical tests

Voxel images have been reconstructed using SMART (simultaneous multiplicative algebraic reconstruction) algorithm. The intensity of the pixel's line of sight was calculated in a form of summation using Eq. (3).

$$P_i = \int_{-\infty}^{\infty} I(x, y, z) ds_i \quad (3)$$

In order to construct the voxel images, the intensity of the pixel's line of sight was converted in a form of discretization using Eq. (4).

$$P_i \approx \sum_j W_{ij} I_j \quad (4)$$

Eq. (5) representing SMART algorithm was used for the generation of voxel images.

$$I_j^{k+1} = I_j^k \prod_i^{N_i} \left[\left(\frac{P_i}{\sum_n W_{in} I_n^k} \right)^{\mu W_{ij}} \right]^{1/N_i} \quad (5)$$

For the calculation of three-dimensional vector map using the voxel images, FFT (fast fourier transformation) cross-correlation method (Wong et al., 2005) was adopted using Eq. (6).

$$F(u, v, \omega) = \frac{1}{WHD} \sum_{x=0}^{W-1} \sum_{y=0}^{H-1} \sum_{z=0}^{D-1} f(x, y, z) e^{-j2\pi(\frac{ux}{W} + \frac{vy}{H} + \frac{\omega z}{D})} \quad (6)$$

Here, W , H , D are the window size for x , y , z coordinates respectively. Phantom ring vortex data were used for the performance test of the constructed tomographic PIV. The displacements of the ring vortex data were generated using Eq. (7).

$$d = \begin{Bmatrix} u \\ v \\ \omega \end{Bmatrix} = \frac{8R}{l} e^{-\left(\frac{R}{l}\right)} \quad (7)$$

Here, R is the distance to the voxel-center ring and l is the width of the vortex. In this study, R was set to 5mm and l was set to 2 mm. To generate the phantom images of the ring vortex, the number of phantom particles was set at from 5,000 to 100,000. The time interval was set to 1/500 seconds. Fig. 5 (a) and Fig. 5(b) show the reference data of the ring vortex and the reconstructed ring vortex calculated by the current tomographic approach, respectively. Fig. 6 shows the experimental schematic of the tomographic system. Four cameras (1280x720, 200fps) were used. For visualization, a continuous laser (8W, 550nm) was used. A rectangular bluff body (30mm x 30mm x 50mm) was set in the water channel over 15mm height from the channel bottom. The Reynolds number was set at 2,000. The measurement volume was set at x -axis (-45mm~50mm), y axis(-25mm~20mm), and z axis(-25mm~25mm). The voxel resolution was set to 1188 x 563 x 625, and the analysis grid was set to 36 x 16 x 18.

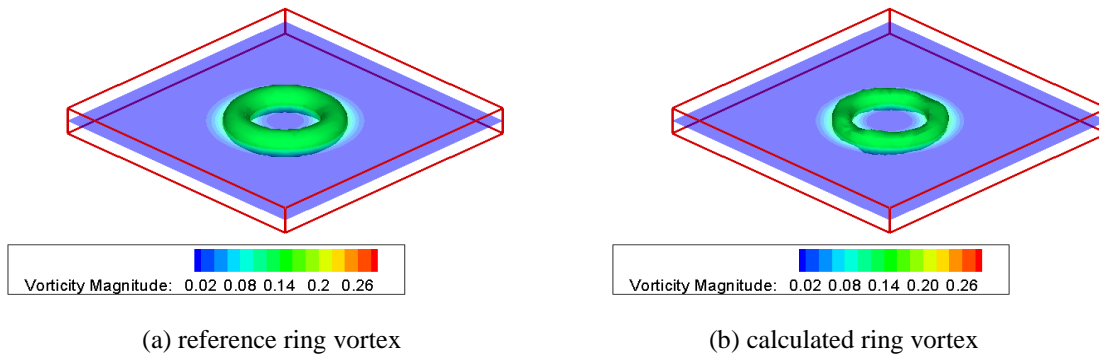


Figure 5: Comparison between the reference and the calculated ring vortex

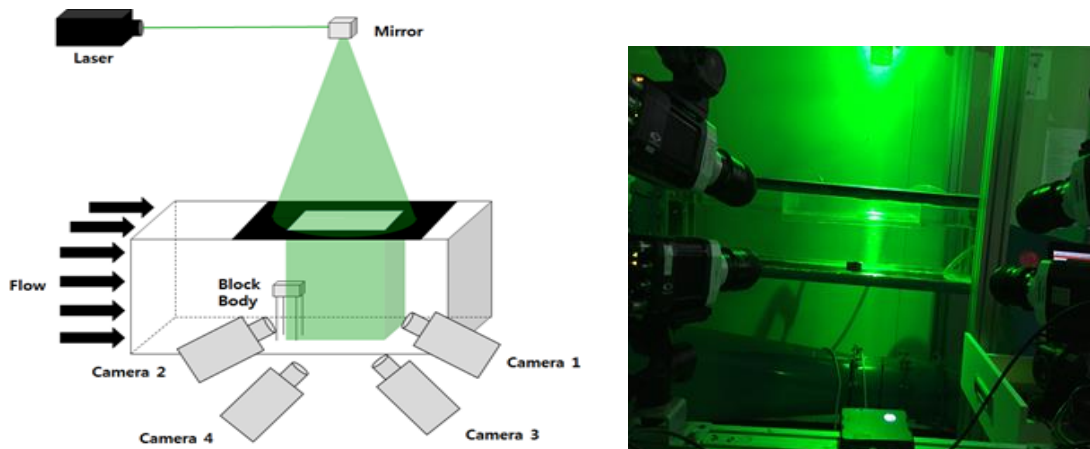


Figure 6: Tomographic PIV system

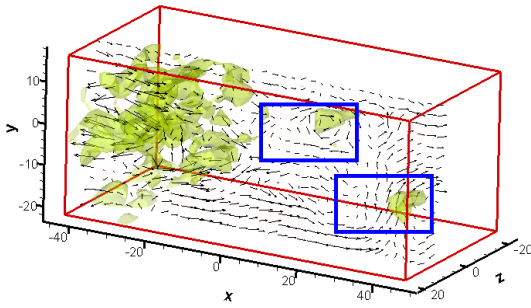


Figure 8: Instantaneous 3D vector map

Figure 7: Experimental setup

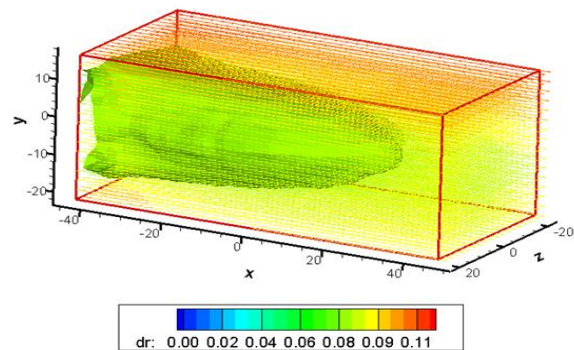


Figure 9: Time mean structure

The voxel size is 64. Fig. 8 and Fig. 9 show the instantaneous and the time mean three-dimensional vector map, respectively obtained by the current tomographic system. Temporal change of the three-dimensional vortex structures has been clearly captured by the constructed tomographic system.

4 Conclusion

The performance of two methods of camera calibrations, 10 parameter method and 11 parameter method (Mapping Function Method), were tested. It was confirmed that the 10 parameter method showed better performance for three-dimensional tomographic approaches. The temporal changes of the wake structures of the rectangular bluff body were quantitatively measured by the constructed tomographic system.

Acknowledgements

This research was supported by Basic Science Research Program through the National Research Foundation of Korea (NRF) funded by the Korea Government (No.2017R1A2B2010603) and (2018R1A2B6009387). Further, this has been also supported by the Supporting Program of Small and Medium Business by SMBA, WC300 R&D (S2415805), and by the Program of Business for Cooperative R&D (R0006261, RFP No. 17-102-006) funded by MOTIE.

References

- Adrian RJ (2005) Twenty years of particle image velocimetry. *Experiments in Fluids* 39:159-169
- Arroyo MP, Greatd, CA (1991) Stereoscopic particle image velocimetry, *Meas. Sci. Technol.*, 2: 1181-1186
- Byrne C (2005) Choosing parameters in block-iterative or ordered subset reconstruction algorithms, *IEEE Trans Image Process* 14(3): 321-327
- Doh DH, Kim DH, Cho KR, Cho YB, Saga T, Kobayashi T (2002) Development of genetic algorithm based 3D-PTV technique, *J. of Visualization* 5(3): 243-254
- Elsinga GE, Scarano F, Wieneke B, Oudheusden BW (2006) Tomographic PIV. *Exp. in Fluids* 41: 933-947
- Malik NA, Dracos TH, Papantoniou DA (1993) Particle tracking velocimetry in three-dimensional flows. Part 2 particle tracking. *Exp. in Fluids* 15:279-294
- Mass HG, Gruen A, Papantoniou DA (1993) Particle tracking velocimetry in three-dimensional flows, Part 1 Photogrammetric determination of particle coordinates. *Exp. in Fluids*, 15: 133-146
- Meng H, Hussain F (1991) Holographic particle velocimetry-a 3D measurement technique for vortex interactions, coherent structures and turbulence. *Fluid Dynamics Res*, 8: 33-52

ICEFM 2018 Munich

Wong JW, Durante C, Cartwright HM (2005) Application of fast fourier transform cross-correlation for the alignment of large chromatographic and spectral datasets. *Anal Chem* 1, 77(17):5655-5561